

# Carbide-free Bainite: Compromise between Rate of Transformation and Properties

Sangeeta Khare\*, Kyooyoung Lee<sup>†</sup> and H. K. D. H. Bhadeshia\*<sup>‡</sup>

\*Graduate Institute of Ferrous Technology (GIFT)  
Pohang University of Science and Technology (POSTECH)  
Pohang 790-784, Republic of Korea

<sup>†</sup>POSCO Technical Research Laboratories  
Gwangyang-shi, Jeonnam 545-090, Republic of Korea

<sup>‡</sup>University of Cambridge  
Materials Science and Metallurgy, Cambridge CB2 3QZ, U.K.

## Abstract

By identifying the relationship between the time required to obtain bainite and parameters such as the transformation temperature and carbon concentration, it has been possible to institute a design procedure which led to the desired mechanical properties and transformation characteristics. The work has also identified difficulties in the calculation of tensile elongation on the basis of a percolation model which suggests that fracture occurs when the fraction of austenite drops below the percolation threshold in the microstructure.

## 1 Introduction

Strong steels based on tempered martensitic microstructures continue to serve well in situations requiring a good combination of strength and toughness [1, 2, 3, 4, 5]. Bainitic steels in this category have not in the past been competitive even though they have the potential of achieving the final structure by continuous cooling transformation, primarily because of the uncontrolled presence of cementite particles. The problem was not resolved by suppressing cementite precipitation using solutes such as silicon, until the realisation that the thermodynamic limit to the extent of transformation that can be achieved also needed to be engineered during alloy design [6, 7]. This latter effect helps avoid large residues of untransformed austenite which can then go on to produce martensite which cracks [6, 7, 8].

Excluding the TRIP-assisted steels where the dominant phase is allotriomorphic ferrite [9, 10, 11, 12, 13], there are therefore two classes of strong steels that have been developed based on

a microstructure consisting of bainitic ferrite, carbon-enriched retained austenite and perhaps some martensite. The first consists of steels whose properties are achieved by continuous cooling transformation [14, 15, 16, 17, 18, 19, 20, 21]. The second is where the hardenability is controlled so that the transformation temperature is dramatically suppressed, giving slender plates of bainitic ferrite, under isothermal conditions [22, 23, 24, 25, 26, 27, 28, 29, 30, 31]. The transformation time in the latter case can, however, be greater than ten days at temperatures as low as 125°C making the process suitable for large components; strength values in excess of 2000 MPa can routinely be achieved.

There is an industrial requirement for the mass production of strong steel-sheet a few mm thick using a continuous process which is rapid and in which the transformation must occur over a narrow temperature range around 350°C, making the process essentially isothermal. The transformation temperature is fixed by the production process and the transformation time must be limited to ten minutes. The ultimate tensile strength should be approximately 1400 MPa with a ductility of about 20%. The purpose of the present work was to see if such a steel can be achieved based on the carbide-free bainitic microstructure described above.

## 2 Feasibility

The short isothermal transformation time is the vital design criterion and to assess whether this can be achieved, data were collected from reported isothermal transformation experiments on carbide-free bainite [7, 32, 22, 33, 34]. The data are plotted in Fig. 1. They correspond to a variety of silicon-rich steels with the carbide-free bainite; much of the variation in the transformation temperature is due to differences in the carbon concentrations of the alloys. The transformation time increase dramatically as the carbon suppresses the transformation temperature. The curves in Fig. 1 are generated by subjecting the data to neural network analysis [35, 36] and the upper and lower curves in each plot represent  $\pm 1\sigma$  modelling uncertainties. Note that the limited data does not deter from using a neural network based on a Bayesian framework in order to identify and plot the uncertainty bounds illustrated. The Bayesian approach used [35, 36] avoids the overfitting which may lead to a modelling of noise in the data.

The shortest time plotted on Fig. 1 is 30 minutes, but the trend indicates that by controlling the chemical composition, it should be feasible to design a steel to comply with the required 10 minutes in the temperature range of interest, and to achieve the required strength. The elongation data show a great deal of scatter so a different procedure will be used to estimate the expected ductility.

## 3 Design

The kinetics of transformation as a function of chemical composition were calculated using a method described elsewhere [37, 38, 39]. In brief, a time-temperature-transformation (TTT) diagram is modelled as consisting of two ‘C’-curves, the one at higher temperatures representing the initiation of reconstructive transformations (allotriomorphic and idiomorphic ferrite, and pearlite), whereas the lower C-curve is for the formation of displacive transformation products such as Widmanstätten

ferrite and bainite. The time period for the initiation of each transformation is calculated using equations based on Russell’s incubation period theory as described in [37]. The steel composition (C, Si, Mn, Ni, Mo, Cr, V, W, Cu) enters into these equations via a free energy change during the nucleation of ferrite from austenite. The lower C–curve has a flat top at a temperature  $T_h$ , which may correspond to the Widmanstätten ferrite–start temperature or the bainite–start temperatures depending on the free energy available [40]. The martensite–start temperature is also calculated thermodynamically, defined by the temperature at which the driving force for diffusionless transformation exceeds the critical value required to trigger nucleation [38, 39]. These calculations define the whole of the initiation part of the TTT diagram and have a reasonable reliability which has been confirmed in a vast number of design experiments including those covering wrought and welding materials based on iron. The computer programs for conducting these calculations are freely available on:

[www.msm.cam.ac.uk/map/mapmain.html](http://www.msm.cam.ac.uk/map/mapmain.html)

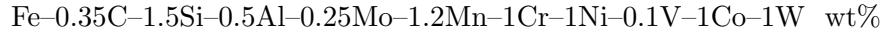
The primary role of the calculations in this work is to define the time period for the onset of the bainite reaction at the required isothermal transformation temperature.

An extensive set of TTT–curve calculations were carried out in which the composition was varied systematically in the range 0–1 Co, 1–2 Cr, 1–2.5 Ni, 1.2–2 Mn, 0–1 W wt%. Silicon and aluminium were fixed at 1.5 and 0.5 wt% respectively in order to control cementite precipitation; aluminium, like cobalt, also helps accelerate the bainite reaction [41, 25]. Carbon has the largest influence in suppressing transformation temperature so its concentration must be kept low enough to be able to achieve the required rate of reaction, but high enough to ensure that the necessary level of strength is achieved. Its concentration was therefore fixed at 0.35 wt%, a value indicated by the data plotted in Fig. 1, particularly the experiments reported in [16, 19] where the mechanical properties achieved are not far from what was required here, but using different heat–treatment conditions. The molybdenum concentration was maintained at 0.25 wt% in order to prevent the embrittlement of austenite grain boundaries by impurities such as phosphorus. A small amount of vanadium (0.1 wt%) was included for austenite grain size control.

The calculation starts by initializing elements as Co(1), Cr(1), Ni(2) and Mn(2) where number in parentheses represents the element concentration in wt% and varying these values systematically in sequence of steps, while keeping other elements C, Si, Mo, Al, V fixed as described above. Fig. 2a is the calculated TTT diagram for composition [0–1]Co–1Cr–2Ni–2Mn with Co varying between 0 to 1 wt%. The value  $Co \approx 1$  wt% was found to accelerate the bainitic transformation and increase the bainitic range ie. the difference between ( $B_S$ ) and ( $M_S$ ) temperatures and thus used as optimum value for the next step. Fig. 2b represents calculated TTT diagram for 1Co–[1–2]Cr–2Ni–2Mn with Cr varying between 1 to 2 wt%. The calculation showed that  $Cr \approx 1$  wt% performs better as compared to  $Cr \approx 2$  wt%. The starting composition therefore for next step in Fig. 2c becomes 1Co–1Cr–[1–2.5]Ni–2Mn with Ni concentration varying between 1 to 2.5 wt%. The value of  $Ni \approx 1$  wt% was found to enhance bainite kinetics and also broadens the bainitic range. By fixing starting composition to 1Co–1Cr–1Ni–[1.2–2]Mn with Mn varying between 1.2 to 2.0 wt% and including tungsten (1 wt%) in this step, a calculated TTT diagram was shown in Fig. 2d. The value of  $Mn \approx 1.2$  wt% further improves the bainitic range and also substantially accelerates the initialization of bainite transformation to lower time.

The summary of various steps of Fig. 2a–d are presented in Fig. 2e where curve ‘A’ represents the highest rate of transformation to bainite with composition 1Co–1Cr–1Ni–1.2Mn–1W while curve

‘B’ represents the lowest rate of transformation having composition 1Cr–2Ni–2Mn and all other alloys have calculated transformation curves fall between these two limits. Given the temperature at which bainite is expected to form, the martensite–start temperature of the alloy must be below 350°C. Curve ‘A’ represents the upper limit of the acceptable amount of alloying permitted to meet this criterion. Clearly, increasing the hardenability of austenite leads to the suppression of transformation temperatures and a reduction in the reaction rate, as indicated by curve ‘B’. The steel corresponding to curve ‘A’ was selected for further investigation; it has the chemical composition:



For this alloy, the calculated initiation of the allotriomorphic ferrite reaction is indicated by curve ‘C’ on Fig. 2e. It appears that the hardenability of this alloy is sufficient to avoid any elevated temperature transformation given that the steel sheet is expected to be cooled at a rate of 5°Cs<sup>-1</sup> in the critical temperature range 700–500°C. The calculated martensite–start temperature is about 330°C.

Judging from Fig. 1, the alloy should achieve the design strength, but it is necessary to estimate the expected elongation. It has been suggested that with microstructures of the kind considered here, failure in a tensile test occurs when the retained austenite loses continuity [42] and that this percolation threshold is reached when the austenite fraction reaches about 0.1. The fraction of austenite present in the initial microstructure can be calculated from the fact that the bainite reaction, in the absence of cementite precipitation, obeys the incomplete–reaction phenomenon [43]. This happens when the carbon concentration in the residual austenite reaches the  $T_0$ ’ curve, which represents the locus of all points on a plot of temperature versus carbon concentration where austenite and ferrite of the same composition have identical free energies after allowing for the stored energy (400 J mol<sup>-1</sup>) of bainite [40]. The austenite remaining at 350°C at the cessation of the bainite reaction,  $V_\gamma^T$ , is given by

$$V_\gamma^T \simeq (\bar{x} - x_\alpha)/(x_{T_0} - x_\alpha) \quad (1)$$

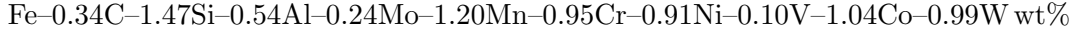
where  $\bar{x}$  is the average carbon concentration,  $x_{T_0}$  is the concentration corresponding to the  $T_0$  curve and  $x_\alpha$  the concentration in ferrite. The residual austenite at 350°C was therefore calculated as  $V_\gamma^T = 0.33$ . Some of this will decompose to martensite on cooling; the fraction  $V_\gamma^0 = 0.24$  retained was calculated using the Koistinen and Marburger equation [44]. The decomposition of the retained austenite as a function of plastic strain was then calculated using a published model [45] which has recently been shown to be the optimum method for such calculations [46]. It is based on the equation

$$\ln V_\gamma^o - \ln V_\gamma = k_1 \Delta G^{\alpha'\gamma} \epsilon \quad (2)$$

where  $V_\gamma^o$  is the fraction of austenite before deformation,  $V_\gamma$  the austenite content as a function of the plastic strain  $\epsilon$ ,  $\Delta G^{\alpha'\gamma}$  the chemical free energy change for transformation without a change in composition (calculated using MTDATA [47]). The constant  $k_1$  has the value 0.002017 mol J<sup>-1</sup> [45]. Fig. 3 shows that percolation is lost when the elongation is approximately 15%.

## 4 Experimental Details

An alloy was made in a vacuum induction furnace, the ingot was reheated to 1200°C for 1 h followed by hot-rolling into 30 mm plate. The chemical composition of the resulting alloy is similar to the intended design:



Cylindrical dilatometric specimens of length 10 mm and diameter 5 mm were subjected to programmed heat-treatments in a BHR DIL805 dilatometer described elsewhere [48].

Tensile testing was conducted on flat samples based on ASTM-E8 geometry (1.5 mm thick, 6 mm wide and 25 mm gauge length) using a Zwick Z600 machine at a crosshead speed of 10 mm min<sup>-1</sup>.

Retained austenite measurements were conducted using CuK<sub>α</sub> X-ray diffraction and Reitveld analysis [49, 50] of the resulting data; details have been described elsewhere [30].

## 5 Results and Discussion

The optical and transmission electron micrographs are presented in Fig. 4; not surprisingly, the microstructure is a routine mixture of platelets of bainitic ferrite embedded in retained austenite.

The martensite-start temperature ( $M_S$ ) of the steel was determined dilatometrically by austenitising at 950°C for 3 min followed by cooling at 20°C s<sup>-1</sup>; the data illustrated in Fig. 5 were analysed using the offset method [48], in which the deviation which identifies the onset of transformation is fixed by calculating the strain corresponding to 1% martensitic transformation in the alloy of interest. From five experiments,  $M_S$  was determined to be 336±10°C, which is consistent with the value calculated as in [38, 39] at 330°C, and indeed with the requirement to produce bainite by isothermal transformation at 350°C.

Fig. 6a shows the corresponding dilatometric data for the isothermal formation of bainite; they show the expected incomplete reaction phenomenon, with the extent of transformation diminishing to zero as the temperature is raised towards the bainite-start temperature. The maximum strain ( $\epsilon$ ) observed was converted into a volume fraction as in [51], so that the carbon concentration of the residual austenite could be determined. The points plotted on Fig. 6b shows that as expected, the reaction ceasing at when carbon concentration in the austenite reaches the  $T'_0$  curve; the discrepancies at low transformation temperatures are expected from the fact that films of austenite trapped between platelets of bainite are able to accumulate more carbon without transforming [52, 53].

The data in Fig.6 were also used to compare the measured transformation kinetics against the calculated time-temperature transformation diagram for the initiation of reaction, assuming that this corresponds to the formation of 0.01 volume fraction of bainite irrespective of the transformation temperature. Fig. 2e shows that the calculations [37] mostly underestimate the time required to form this fraction of bainite; the reason for this discrepancy is not clear.

Fig. 7a shows plots of engineering stress versus engineering strain for three tensile test samples; the recorded values of ultimate tensile strength and total elongation are found to be 1452–1457 MPa and 12–15% respectively; the uniform elongation is 7–8%. The measured total elongation is close to that calculated using the percolation model at 15% in Fig. 3. The calculation was based on  $V_\gamma^\circ$  estimated to be 0.24 using equation 1. The same equation using the experimental value of  $x_\gamma$  (Fig. 6b) rather than  $x_{T_0}$  yields  $V_\gamma^T = 0.22$  and since the martensite–start temperature is suppressed to  $-37^\circ\text{C}$ ,  $V_\gamma^\circ = V_\gamma^T$ . Curve ‘a’ in Fig. 8 shows the consequent change in the strain–induced transformation behaviour indicating that the elongation to be expected should be 25% because of the increased thermodynamic stability of the austenite.

Curve ‘b’ on Fig. 8 is calculated using an X–ray diffraction determined value of  $V_\gamma^\circ = 0.17$ ; the diffraction experiment was repeated twice to confirm that the fraction of retained austenite is between 0.17–0.18. With this, the predicted elongation at 16% is closer to the measured values in the range 12–15%.

The carbon concentrations of the residual austenite in Fig. 6b were derived from the corresponding dilatometric curves by converting the maximum observed dilatation at any temperature into a fraction of transformation, and then using mass balance, into  $x_\gamma$  [51]. This involves a calculation of the lattice parameters of the austenite and ferrite as a function of the solute concentration and temperature. For  $350^\circ\text{C}$ , the parameter for the carbon–enriched residual austenite at the point of maximum transformation strain was calculated to be  $3.6512 \text{ \AA}$ , which is calculated using thermal expansivity measurements to contract to  $3.6236 \text{ \AA}$  at ambient temperature. The latter is reasonably consistent with the X–ray determined lattice parameter of the retained austenite at  $3.6175 \pm 0.001 \text{ \AA}$ . This gives confidence in the interpretation of the dilatometrically determined  $x_\gamma = 1.47 \text{ wt}\%$  which at most may be an overestimation by  $0.18 \text{ wt}\%$  if the X–ray determined lattice parameter is used. If the X–ray measurement is taken to be more accurate, then the martensite–start temperature of  $V_\gamma^T$  would rise to  $20^\circ\text{C}$  so that martensite would not form on cooling the sample to room temperature; this does not strictly explain the discrepancy between the values of  $V_\gamma^\circ$  for curves ‘a’ and ‘b’ illustrated in Fig. 8. The explanation consistent with past experience [54] is that the carbon is not uniformly distributed, with the larger islands containing a lower concentration and hence decomposing to martensite on cooling.

It follows that one difficulty in calculating the fracture strain is the estimation of the fraction and stability of the austenite, given that the latter phase is unlikely to be homogeneous in terms of both size and carbon concentration. A second feature neglected in the percolation analysis is that the macroscopic strain will not in the later stages of deformation be uniform given the onset of necking in a tensile test. A further analysis was done to examine the consequences of the latter effect by comparing the local strain at the neck to the value measured over a gauge length of 25 mm. Fig. 7b shows the fractured tensile specimen; there was virtually zero plastic strain in the  $z$  direction with the failure typical of thin samples via shear on the plane containing  $y$  and inclined at  $45^\circ$  to  $x$ . The contraction strain along  $y$  at the arrowed position of fracture was  $\epsilon_y = -17\%$ , which because  $\epsilon_z$  is zero, corresponds to an elongation along the tensile axis of  $\epsilon_x = 17\%$ , which is only slightly larger than the 15% recorded over the whole gauge length (*cf.* calculated value of 16%). It is concluded therefore that in the present case the necking does not significantly influence the outcome of the percolation analysis because of the thin–sheet shape of the specimen.

As a precautionary comment, it is worth emphasising that the fracture strain as a generic issue

depends not only on the occurrence of necking, but also on the damage sites and rate of occurrence. The austenite clearly has a role in determining ductility, but the relationship of ductility and the quantity of retained austenite cannot in general be straightforward.

## 6 Conclusions

By assessing literature data on the relationship between transformation time and mechanical properties, it has been possible with the help of design procedure to obtain in the first iteration, a steel which has the desired microstructure of carbide-free bainitic ferrite and carbon-enriched retained austenite. Furthermore, the structure can, as required, be obtained by isothermal transformation for ten minutes, and has been shown experimentally to have the intended properties.

The work has also identified detailed discrepancies in the calculation of time-temperature-transformation diagrams and in the estimation of elongation. These topics will be the subject of continued research.

## Acknowledgments

We are grateful to Professor Hae-Geon Lee of the Graduate Institute of Ferrous Technology for the provision of laboratory facilities at POSTECH, and to POSCO for help and support.

## References

- [1] M. J. May, T. Gladman, E. F. Walker: *Philosophical Transactions of the Royal Society*, London 1976, vol. 282A, pp. 377–387.
- [2] W. M. Imrie: *Philosophical Transactions of the Royal Society*, London 1976, vol. 282A, pp. 91–104.
- [3] W. M. G. Jr.: *Journal of Metals* 1990, vol. 42, pp. 20–24.
- [4] Y. Tomita: *Materials Science and Technology* 1991, vol. 7, pp. 481–489.
- [5] G. Luxemburger, M. Bockelmann, P. Wolf, F. Hanus, R. Cawelius, J. Buchholz: *International Journal of Pressure Vessels and Piping* 2004, vol. 81, pp. 159–171.
- [6] H. K. D. H. Bhadeshia, D. V. Edmonds: *Metal Science* 1983, vol. 17, pp. 411–419.
- [7] H. K. D. H. Bhadeshia, D. V. Edmonds: *Metal Science* 1983, vol. 17, pp. 420–425.
- [8] S. Chatterjee, H. K. D. H. Bhadeshia: *Materials Science and Technology* 2006, vol. 22, pp. 645–649.
- [9] O. Matsumura, Y. Sakuma, H. Takechi: *Transactions of the Iron and Steel Institute of Japan* 1987, vol. 27, pp. 570–579.

- [10] O. Matsumura, Y. Sakuma, H. Takechi: *Scripta Metallurgica* 1987, vol. 27, pp. 1301–1306.
- [11] Y. Sakuma, O. Matsumura, H. Takechi: *Metallurgical & Materials Transactions A* 1991, vol. 22, pp. 489–498.
- [12] P. J. Jacques: *Current Opinion in Solid State and Materials Science* 2004, vol. 8, pp. 259–265.
- [13] B. DeCooman: *Current Opinion in Solid State and Materials Science* 2004, vol. 8, pp. 285–303.
- [14] N. Jin, P. Clayton: *Wear* 1997, vol. 202, pp. 202–207.
- [15] F. G. Caballero, H. K. D. H. Bhadeshia, K. J. A. Mawella, D. G. Jones, P. Brown: *Materials Science and Technology* 2001, vol. 17, pp. 512–516.
- [16] F. G. Caballero, H. K. D. H. Bhadeshia, K. J. A. Mawella, D. G. Jones, P. Brown: *Materials Science and Technology* 2001, vol. 17, pp. 517–522.
- [17] Z. G. Yang, H. S. Fang: *Current Opinion in Solid State and Materials Science* 2005, vol. 9, pp. 277–286.
- [18] H. S. Fang, Z. L. Tan, B. Z. Bai: *Journal of Iron and Steel Research International* 2005, vol. 12, pp. 1–10.
- [19] F. G. Caballero, M. J. Santofimia, C. Capdevila, C. Garcia-Mateo, C. G. de Andrés: *ISIJ International* 2006, vol. 46, pp. 1479–1488.
- [20] M. R. Zhang, H. C. Gu: *Materials Science and Technology* 2007, vol. 23, pp. 970–974.
- [21] F. G. Caballero, C. G. Mateo, J. Chao, M. J. Santofimia, C. Capdevila, C. G. de Andrés: *ISIJ International* 2008, vol. 48, pp. 1256–1262.
- [22] F. G. Caballero, H. K. D. H. Bhadeshia, K. J. A. Mawella, D. G. Jones, P. Brown: *Materials Science and Technology* 2002, vol. 18, pp. 279–284.
- [23] C. Garcia-Mateo, F. G. Caballero, H. K. D. H. Bhadeshia: *ISIJ International* 2003, vol. 43, pp. 1238–1243.
- [24] P. M. Brown, D. P. Baxter: *Hyper-strength bainitic steels: in: Materials Science and Technology 2004: TMS, Warrendale, Pennsylvania, USA, 2004: pp. 433–438.*
- [25] C. Garcia-Mateo, F. G. Caballero, H. K. D. H. Bhadeshia: *ISIJ International* 2003, vol. 43, pp. 1821–1825.
- [26] M. Peet, S. S. Babu, M. K. Miller, H. K. D. H. Bhadeshia: *Scripta Materialia* 2004, vol. 50, pp. 1277–1281.
- [27] M. Peet, C. Garcia-Mateo, F. G. Caballero, H. K. D. H. Bhadeshia: *Materials Science and Technology* 2004, vol. 20, pp. 814–818.
- [28] K. Goa, L. D. Wang, M. Zhu, J. D. Chen, Y. J. Shi, M. K. Kang: *Acta Metallurgica Sinica* 2007, vol. 43, pp. 315–320.
- [29] H. K. D. H. Bhadeshia: *Materials Science and Technology* 2005, vol. 21, pp. 1293–1302.

- [30] H.-S. Yang, H. K. D. H. Bhadeshia: *Materials Science and Technology* 2008, vol. 24, pp. 335–342.
- [31] F. C. Zhang, T. S. Wang, P. Zhang, C. L. Zhang, B. Lv, M. Zhang, Y. Z. Zhang: *Scripta Materialia* 2008, vol. 59, pp. 294–296.
- [32] L. C. Chang: *Wear* 2005, vol. 258, pp. 730–743.
- [33] C. G. Mateo, F. G. Caballero: *ISIJ International* 2005, vol. 45, pp. 1736–1740.
- [34] V. T. T. Miihkinen, D. V. Edmonds: *Materials Science and Technology* 1987, vol. 3, pp. 432–440.
- [35] D. J. C. MacKay: *Neural Computation* 1992, vol. 4, pp. 448–472.
- [36] D. J. C. MacKay: *ASHRAE Transactions* 1994, vol. 100, pp. 1053–1062.
- [37] H. K. D. H. Bhadeshia: *Metal Science* 1982, vol. 16, pp. 159–165.
- [38] H. K. D. H. Bhadeshia: *Metal Science* 1981, vol. 15, pp. 175–177.
- [39] H. K. D. H. Bhadeshia: *Metal Science* 1981, vol. 15, pp. 178–150.
- [40] H. K. D. H. Bhadeshia: *Acta Metallurgica* 1981, vol. 29, pp. 1117–1130.
- [41] H. I. Aaronson, H. A. Domian, G. M. Pound: *TMS–AIME* 1966, vol. 236, pp. 781–796.
- [42] H. K. D. H. Bhadeshia: *Materials Science and Engineering A* 2008, vol. 481–482, pp. 36–39.
- [43] H. K. D. H. Bhadeshia, D. V. Edmonds: *Acta Metallurgica* 1980, vol. 28, pp. 1265–1273.
- [44] D. P. Koistinen, R. E. Marburger: *Acta Metallurgica* 1959, vol. 7, pp. 59–60.
- [45] M. Sherif, C. Garcia-Mateo, T. Sourmail, H. K. D. H. Bhadeshia: *Materials Science and Technology* 2004, vol. 20, pp. 319–322.
- [46] M. Mukherjee, T. Bhattacharyya, S. B. Singh: Models for austenite to martensite transformation in TRIP aided steels: A comparative study: in: S. K. Chaudhuri, B. K. Jah, S. Srikant, P. K. Maini, A. Deva, R. Datta (Eds.), *Thermomechanical simulation and processing of steels: Allied Publishers Pvt. Ltd., New Delhi, India, 2008: pp. 352–362.*
- [47] NPL: MTDATA: Software, National Physical Laboratory, Teddington, U.K. 2006,.
- [48] H.-S. Yang, H. K. D. H. Bhadeshia: *Materials Science and Technology* 2007, vol. 23, pp. 556–560.
- [49] H. M. Rietveld: *Acta Crystallographica* 1967, vol. 22, pp. 151–152.
- [50] H. M. Rietveld: *Journal of Applied Crystallography* 1969, vol. 2, pp. 65–71.
- [51] H. K. D. H. Bhadeshia, S. A. David, J. M. Vitek, R. W. Reed: *Materials Science and Technology* 1991, vol. 7, pp. 686–698.
- [52] P. G. Self, H. K. D. H. Bhadeshia, W. M. Stobbs: *Ultramicroscopy* 1981, vol. 6, pp. 29–40.
- [53] H. K. D. H. Bhadeshia, A. R. Waugh: *Acta Metallurgica* 1982, vol. 30, pp. 775–784.
- [54] S. J. Matas, R. F. Hehemann: *TMS–AIME* 1961, vol. 221, pp. 179–185.

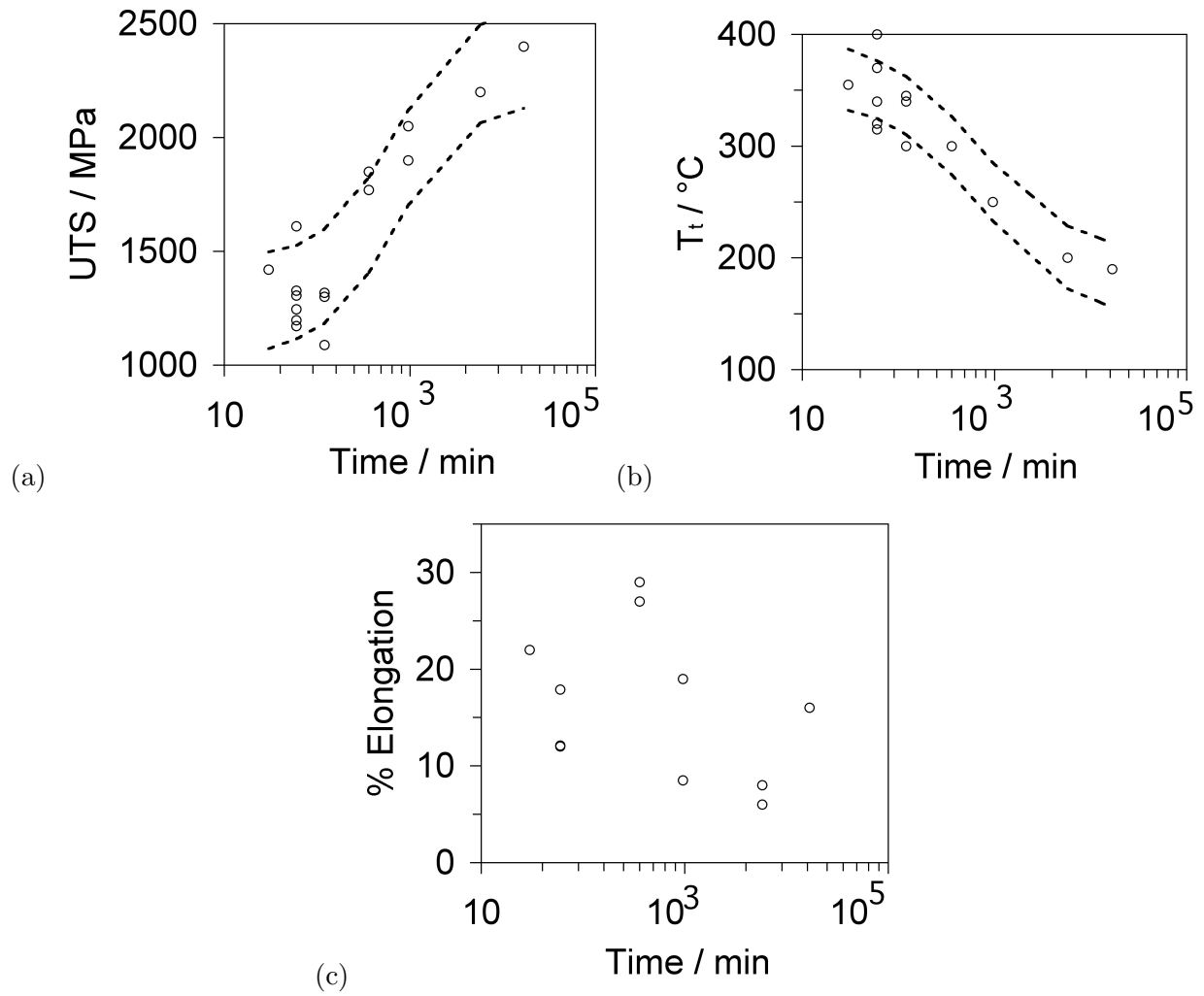


Figure 1: Published experimental data (points) [7, 32, 22, 33, 34] as a function of transformation time. The curves represent  $\pm 1\sigma$  confidence limits obtained by subjecting the data to a neural network analysis. (a) Ultimate tensile strength (UTS) as a function of isothermal transformation time. (b) Transformation temperature ( $T_t$ ) as a function of isothermal transformation time. (c) Elongation as a function of isothermal transformation time.

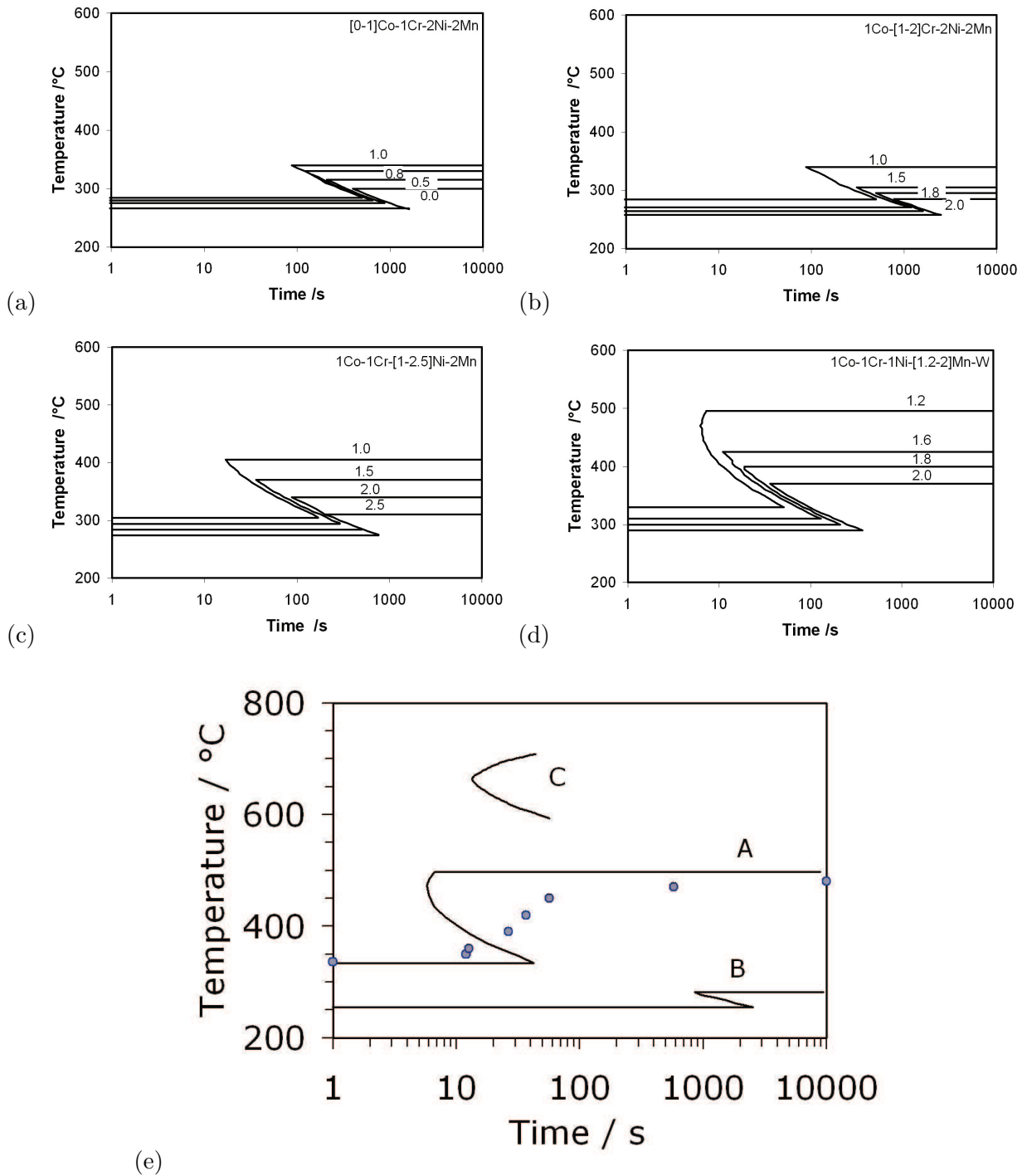


Figure 2: Calculated time–temperature–transformation curves for the initiation of transformation. (a) Effect of cobalt in alloy containing 1Cr–2Ni–2Mn wt%. (b) Effect of chromium in alloy containing 1Co–2Ni–2Mn wt%. (c) Effect of nickel in alloy containing 1Co–1Cr–2Mn wt%. (d) Effect of manganese in alloy containing 1Co–1Cr–1Ni–1W wt%. (e) Curves ‘A’ and ‘B’ refer to highest and lowest rate of bainite transformation whereas ‘C’ describes the formation of allotriomorphic ferrite. The points are experimental data described later.

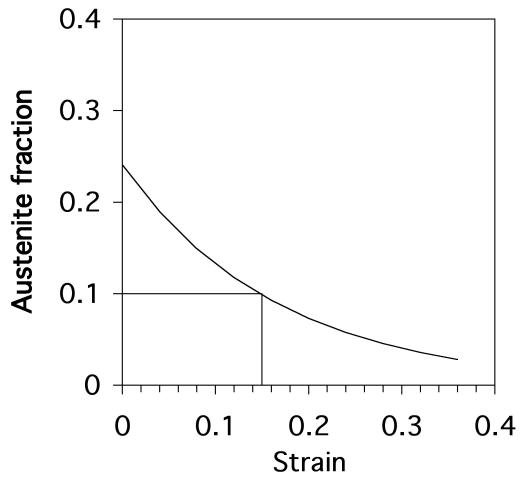


Figure 3: Calculated decrease in retained austenite content as a function of plastic strain.

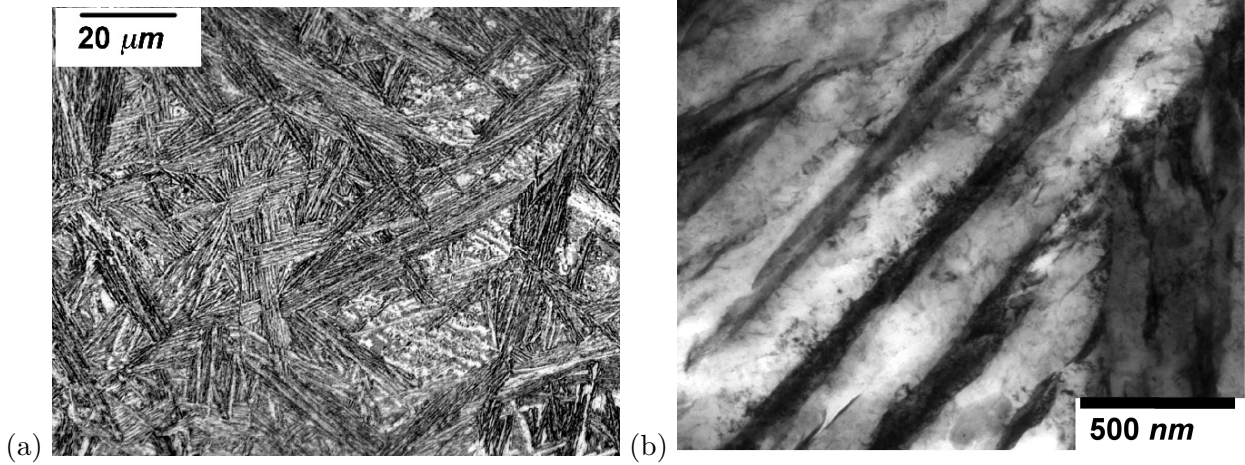


Figure 4: Optical and transmission electron micrographs of the structure obtained by isothermal transformation at 350°C for ten minutes.

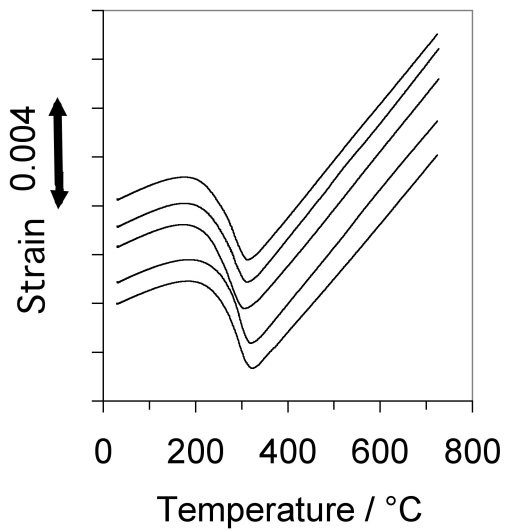


Figure 5: Martensite-start temperature measurements.

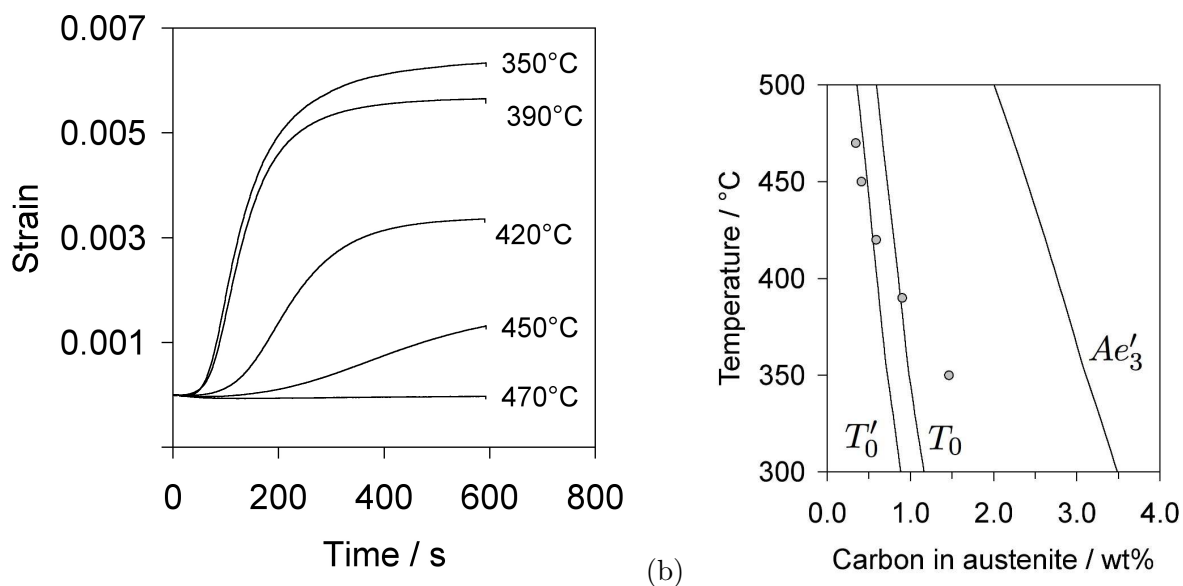


Figure 6: (a) Isothermal transformation curves. (b) Calculated  $T'_0$ ,  $T_0$  and the paraequilibrium  $Ae'_3$  curve, together with experimental data (points) showing the carbon concentration at which the bainite reaction ceases.

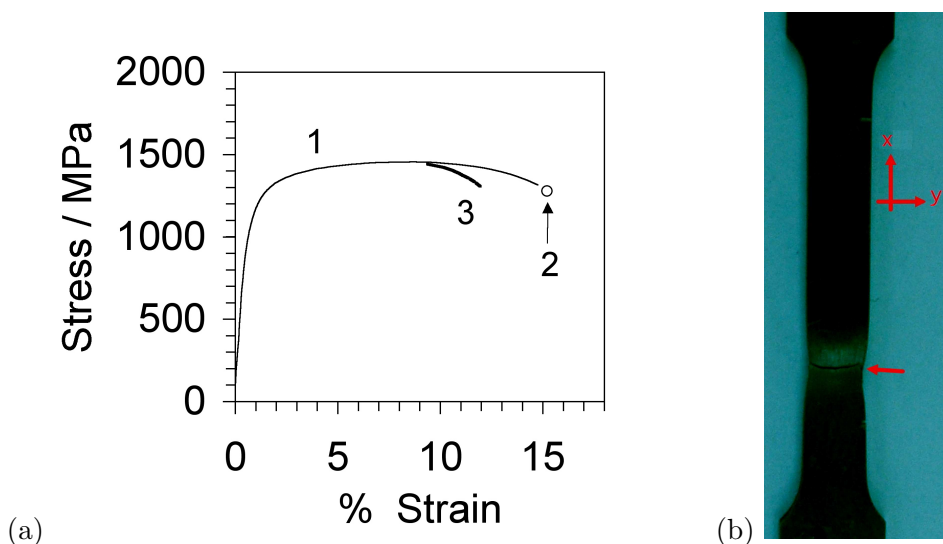


Figure 7: (a) Three engineering stress versus engineering strain curves. Curve 1 is plotted in full, curve 2 is almost identical so only the final point corresponding to failure is plotted. (b) The tensile test sample after fracture.

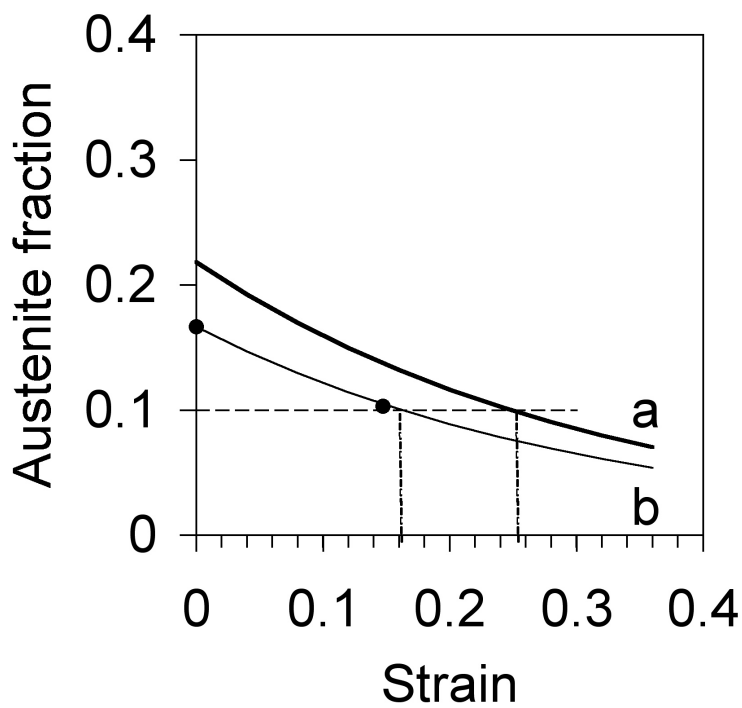


Figure 8: Calculations of strain-induced transformation of austenite assuming (a) dilatometrically determined  $V_{\gamma}^{\circ} = 0.22$  and (b) X-ray determined  $V_{\gamma}^{\circ} = 0.17$ . The points correspond to measured values.